BOREAL ENVIRONMENT RESEARCH 21: 44–52
ISSN 1239-6095 (print) ISSN 1797-2469 (online)

Helsinki 8 April 2016

A note on ADCP-based indirect observations of turbulence

Linda Enmar[1)], Iréne Lake[2)], Peter Lundberg[1)] and Peter Sigray[1)3)]*

[1)] *Department of Meteorology/Physical Oceanography, Stockholm University, SE-10691 Stockholm, Sweden(*corresponding author's e-mail: peters@misu.su.se)*
[2)] *Swedish Meteorological and Hydrological Institute, SE-60176 Norrköping, Sweden*
[3)] *Swedish Defence Research Agency, SE-16490 Stockholm, Sweden*

Received 25 Sep. 2014, final version received 28 May 2015, accepted 25 Aug. 2015

Enmar L., Lake I., Lundberg P. & Sigray P. 2016: A note on ADCP-based indirect observations of turbulence. *Boreal Env. Res.* 21: 44–52.

A 70-day data set from bottom-mounted ADCPs on the two sides of the Faroe-Bank Channel was analysed using the recorded flow variance and echo intensity in the deeper reaches of the passage as proxies for turbulence. A consistent picture emerged, not least since the data losses (which were ascribed to turbulence-induced activation of the fish-elimination option in the ADCP software) could be shown to co-vary with the internal M_2 tide affecting the vertical shear, which in turn proved to be correlated with the flow variance.

Introduction

Most investigations concerned with ADCP observations of turbulence dealt with the bottom boundary layer (*see* e.g. Lorke and Wüest 2005, Perlin *et al*. 2007). Here we instead focus on processes at a considerable distance from solid boundaries, something which has been subjected to less attention. The present study was based on a data set from the deeper reaches of the Faroe-Bank Channel (*see* Fig. 1), where bottom-mounted ADCPs have been deployed at the passage threshold since the mid-1990s to monitor the deep-water overflow from the Norwegian Sea (Hansen and Østerhus 2007).

The aim of the investigation was not to present quantitative data on the mixing taking place in this passage connecting the deep regions of the Norwegian Sea with the North Atlantic; this question has been dealt with in an expert fashion by Mauritzen *et al*. (2005) as well as by Fer *et al*. (2010, 2014), all the three studies having their primary focus on the turbulent characteristics of the descending deep-water plume somewhat downstream of the Faroe-Bank Channel threshold. The intent of the present study was rather to demonstrate how a somewhat novel application of ADCP technology possibly can serve as a contribution to a deeper understanding of oceanic turbulence.

Editor in charge of this article: Kai Myrberg

General description of the experimental site and data set

The observational material used for this investigation consists primarily of records from ADCPs at locations on the two sides of the Faroe-Bank-Channel sill: the northeastern site denoted NWFA (61°26.409´N, 8°14.560´W; bottom depth 770 m) and the southwestern site denoted NWFC (61°23.609´N, 8°18.957´W; bottom depth 840 m). Observations were made every 20 minutes from 12:00 on 4 July to 21:00 on 11 September 1998. The bottom-mounted, upward-looking ADCPs were of the four-beam

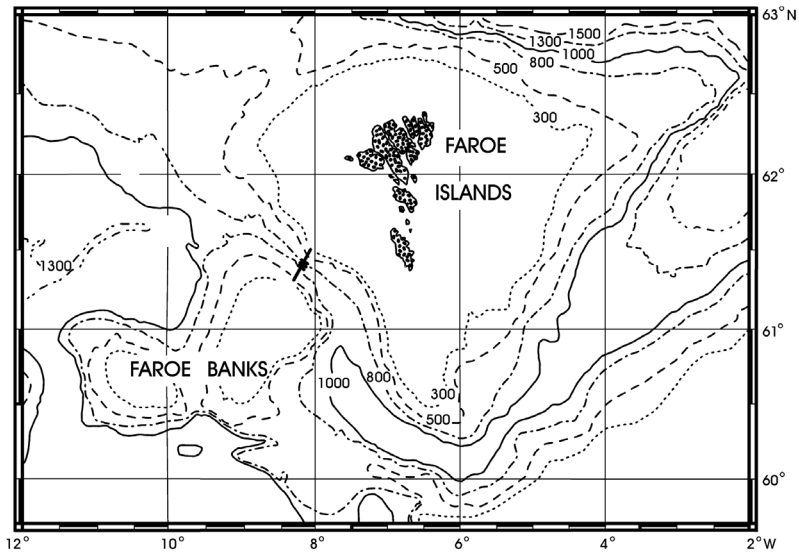

Fig. 1. The Faroe region with experimental site on the sill of the Faroe-Bank Channel. The black line southwest of the Faroe Islands shows the experimental site.

75-kHz RDI broadband variety and operated in single-ping mode. Bin heights were 25 m, and thus the observational ranges extended well into the upper-layer water masses. This spatio-temporal resolution is insufficient for conventional turbulence studies; it was dictated by the main purpose of the experiment, namely to facilitate the establishment of precise deep-water-transport estimates. The ADCP data set nevertheless appeared to be relevant for a qualitative discussion of turbulence.

The overall hydrography in the Faroe-Bank Channel is characterized by a "two-layer" stratification with a more-or-less passive upper layer of North Atlantic water overlying a rapidly moving (0.8–1.4 m s^{-1}) body of cold, low-saline deep water originating from the Norwegian Sea. The isotherm distribution across the sill on 4 July 1998 when the ADCPs were deployed is depicted in Fig. 2. Since in the Faroe region the relation between temperature and density is one-to-one (Borenäs and Lundberg 1988), it is recognized that the deep-water flow is geostrophically balanced. Although not evident from Fig. 2, in general the isotherms are "pinched" towards the southwest and more spread out on the Faroe side of the passage (cf. Johnson and Sanford 1992, Borenäs *et al*. 2001). The upper and lower water masses are separated by a shear layer, which, consonant with the stratification, is less pronounced towards the northeast.

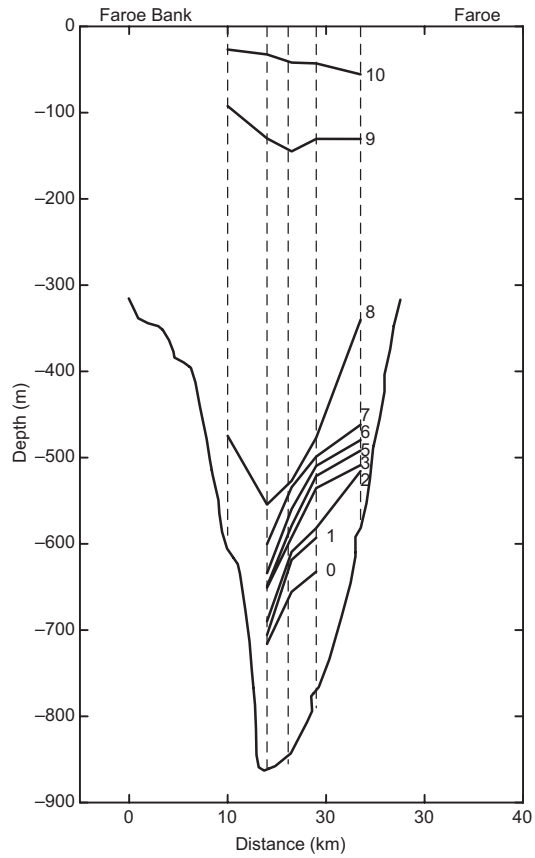

Fig. 2. Isotherm distribution across the Faroe-Bank Channel threshold on 4 July 1998 when the ADCPs were deployed.

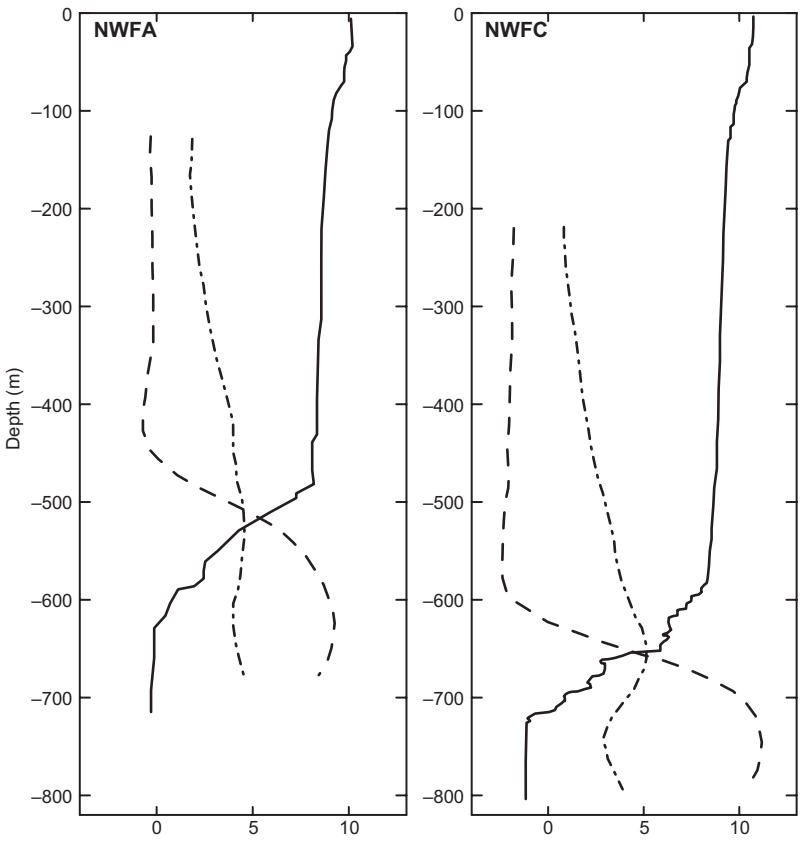

Fig. 3. Vertical profiles of temperature (°C, solid line), along-channel velocity divided by 10 (cm s^{-1}, dashed line) and the backscatter intensity in arbitrary units (dash-dotted line) at the ADCP stations NWFC and NWFA on the two sides of the passage on 4 July 1998. The temperature profiles were obtained from CTD casts made when the ADCPs were deployed, whereas the velocity and acoustical data were recorded by the ADCPs.

As expected on dynamical grounds, the maximum density gradient coincided with the strongest vertical shear (*see* also Lake *et al*. 2005), at which level also high back-scatter intensities were found (the latter feature particularly evident at site NWFC; *see* Fig. 3). The hydrographic situation illustrated by the temperature profiles (*see* Fig. 3) is typical (Borenäs and Lundberg 2004) for the deep waters of the passage; at the northeastern site NWFA stratified conditions extend all the way to the bottom, whereas at NWFC on the southwestern side of the passage an extremely sharp pycnocline was present, below which a homogeneous water mass of purely Norwegian-Sea origin extended all the way to the seabed. As is evident from the analysis of the ADCP records presented below, this contrast between the hydrographic conditions at the two sides of the passage has significant consequences for the results to be reported in this study.

Unfortunately, the only available hydrographic data are those from the initial series of CTD casts made when the current instruments were deployed, and thus the 70-day observational material was heavily skewed in favour of the ADCP records. The fact that the zone of maximum vertical shear is associated with the pycnocline nevertheless permitted some indirect conclusions about the stratification.

Analysis

The observed velocities were treated in component form: v was taken to be orientated in the local cardinal direction of the passage (304°), u and w in the cross-channel and vertical directions, respectively. Estimates of the flow variance were obtained by separating the observed velocities into the mean and fluctuating parts, $(u,v,w) = (\overline{u},\overline{v},\overline{w}) + (u',v',w')$, and determining $u'^2 + v'^2 + w'^2$. As evidenced by the results presented in Fig. 4, at NWFA the variances were generally lower and their distribution was less

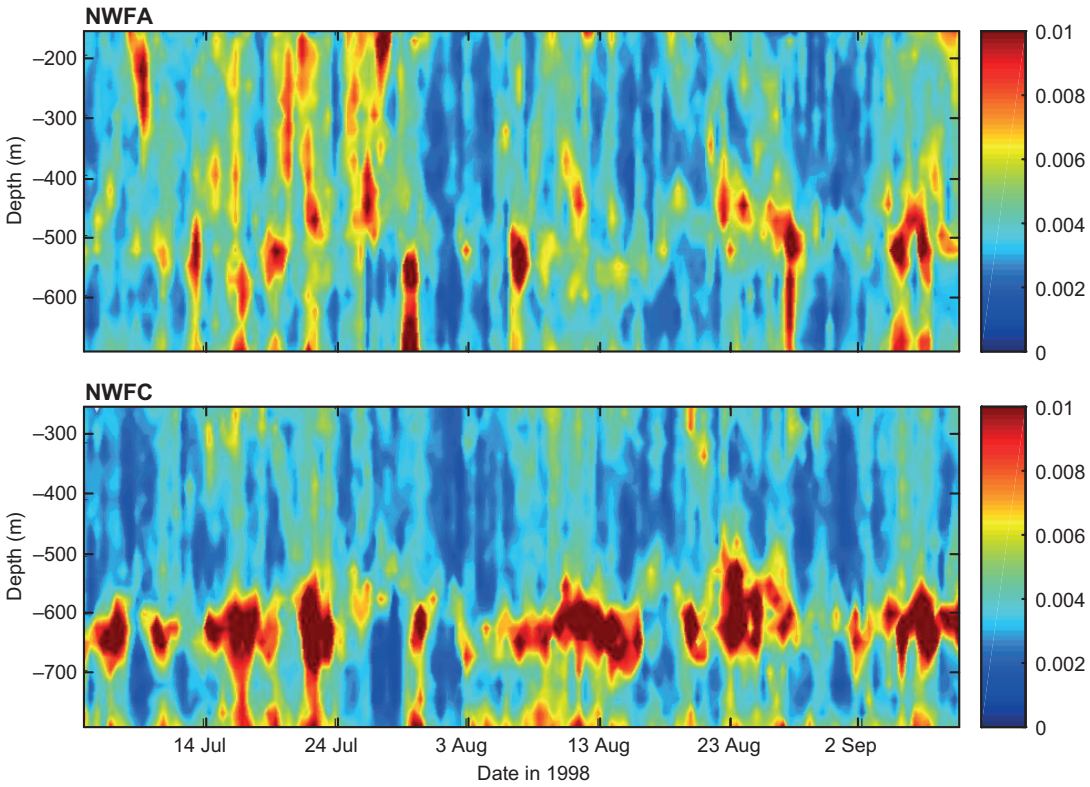

Fig. 4. Time evolution of the variance distribution over depth calculated using a 3-hour window at the NWFA and NWFC sites during the 70-day experiment.

distinct (these results remained unchanged when 6- and 9-hour averaging was applied), and the highest variances appear to be located more-or-less at the maximum-shear level. This is further confirmed by the time evolution of the depths of maximum variance and vertical shear at the two ADCP stations during the 70-day intensive-study period (Fig. 5). On the southwestern side of the passage (NWFC), both maxima tend to be found at the same level (correlation 0.77), except a minor number of excursions. At NWFA, the correspondence was less pronounced with a correlation of 0.68, mirroring the more diffuse stratification and shear zone characterizing the northeastern side of the passage (cf. Fig. 3).

The strongest echo returns at site NWFC were found at the level of maximum vertical shear (which may be identified with the pycnocline) (*see* Fig. 3), a feature which was less pronounced at NWFA with its weaker stratification. Generally acoustic back-scatter is assumed to originate from particulate and biological matter in the water column. The deeper regions of the Faroe-Bank Channel are, however, characterized by scarcity of biological life as well as a dearth of fine-grained particulate matter since the seabed is well-scoured by the rapid current (cf. Nörrevang *et al*. 1994). Additionally the ADCP working frequency of 75 kHz is ill adapted for detecting *Calanus finnmarchicus*, the dominant copepod in the Faroe region (S. Kaartvedt pers. comm.). It thus appears likely that a significant part of the observed acoustic back-scatter originates from refractive-index fluctuations due to turbulence acting in concert with a significant thermal gradient (Goodman 1990, Seim *et al*. 1995).

The depth distribution of the back-scatter intensities at NWFC (Fig. 6) shows a well-delimited band of high intensities around the shear zone, whereas NWFA is predominantly characterized by comparatively high intensities from the shear zone all the way to the bottom. The explanation is that at NWFC (*see* Fig. 3),

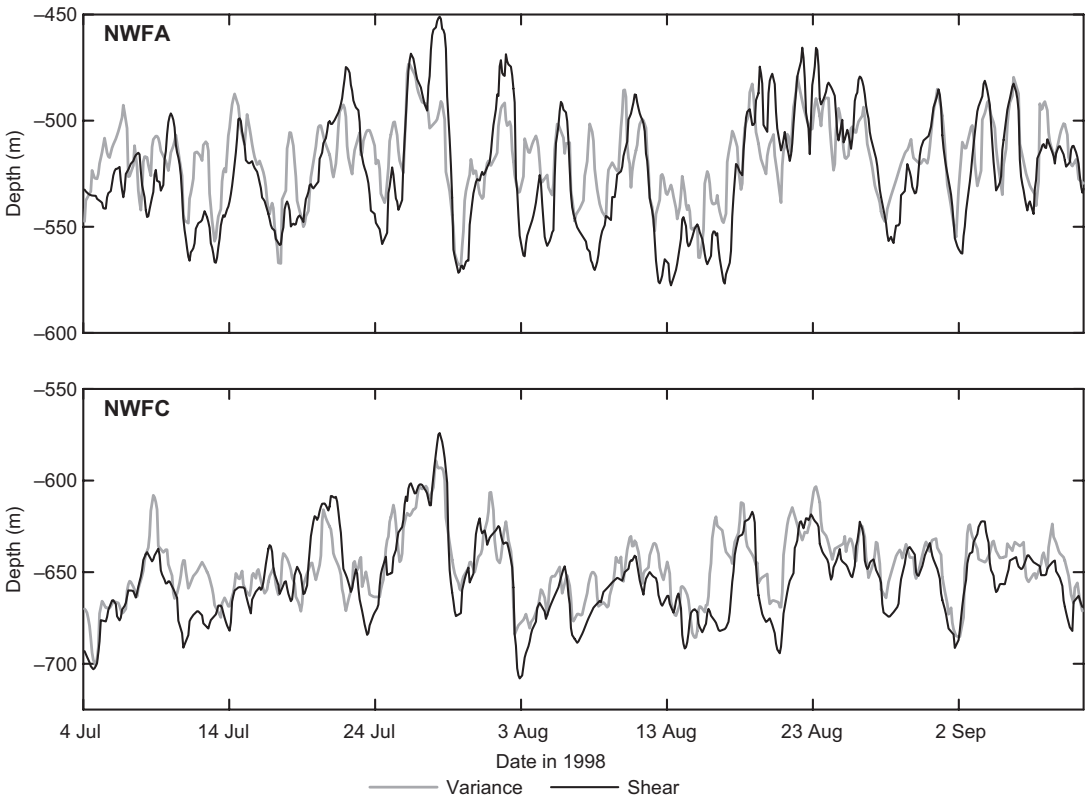

Fig. 5. Observed levels of maximum shear and maximum variance based on a 3-hour window at the NWFA and NWFC sites. Both sets of results smoothed over 12 hours.

the deep water is almost thermally homogeneous below approximately 700 m and hence refractive-index fluctuations cannot be expected here. At NWFA, on the other hand, the thermal stratification extends all the way to the bottom and hence turbulence-induced fluctuations of the refractive index are capable of giving rise to comparatively high back-scatter intensities here. Note, however, the anomalous conditions at NWFA on 27/28 July when a large pulse of more-or-less unadulterated Norwegian Sea deep water passed the transect, as described by Lake *et al*. (2005).

To investigate these acoustical features more closely, the "raw-data" back-scatter intensities at the pycnocline/level of maximum vertical shear were extracted from each velocity profile. Hereafter, a standard depth-dependent compensation was made for beam spreading and sound absorption (cf. Thomsen *et al*. 1989). Since the magnitudes of the back-scatter intensities from the two ADCPs are not directly comparable, the cluster properties may instead be judged on the basis of a least-squares fit (cf. the regression lines in Fig. 7). (The norms of the residuals were comparable: 416 and 420 at NWFA and NWFC, respectively. A similar analysis of the "raw" intensities yielded residuals of 546 and 501; the beam-spreading and sound-absorption compensation evidently served a useful purpose.) As seen in Fig. 7, the results for NWFC not only comprise a large number of spatially highly distinct acoustic returns, but also show the strongest functional dependence (i.e. regression-line slope) of the return intensity on the magnitude of the shear/"density gradient". This dependence is not surprising in view of the fact that a stronger shear is associated with a larger density contrast (which, since it primarily is temperature-governed, in turn is conducive for refractive-index fluctuations). At NWFA with its weaker stratification, the less pronounced thermal and velocity

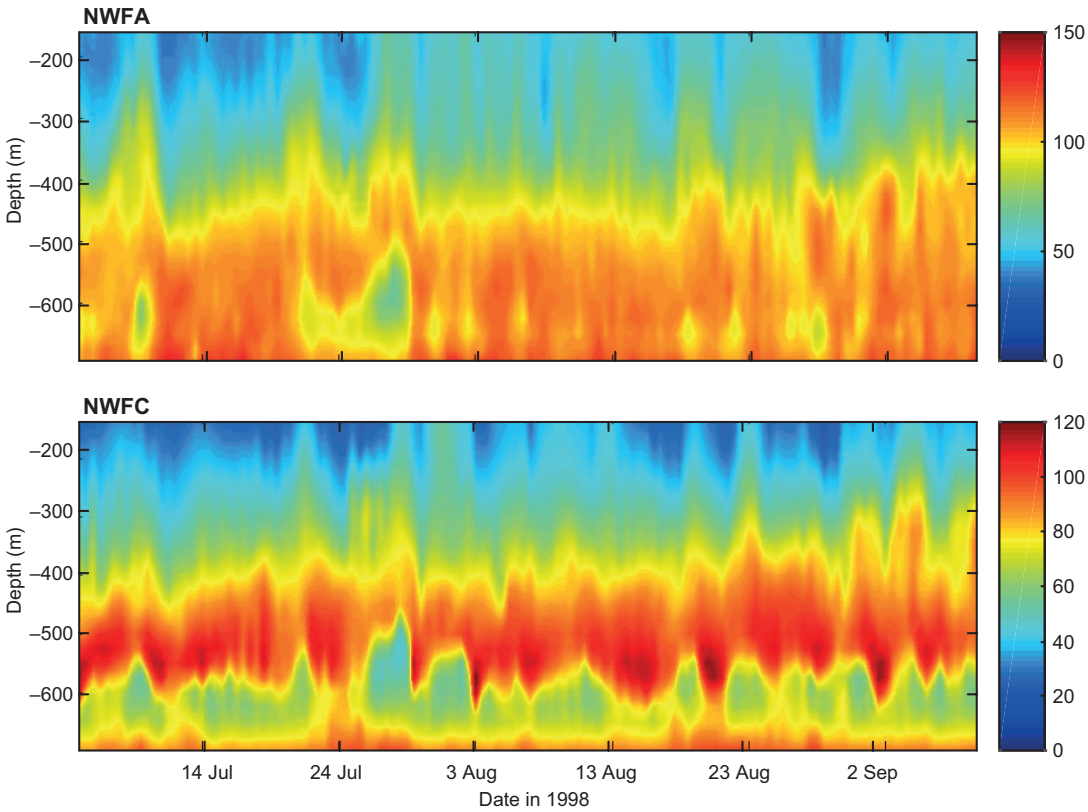

Fig. 6. The evolution in time of the depth distribution of the back-scatter intensities at the NWFA and NWFC sites. It is of no consequence that the intensity scales on the right-hand side of the figure differ as ADCPs do not provide intensities in absolute terms, but only relative.

gradients analogously give rise to a diminished shear-dependence (*viz*. a smaller slope of the regression line) of the return intensities (as well as an only minuscule number of spatially highly distinct return echoes).

Data losses

An interesting feature of the records is that data losses (frequently in the form of single-bin observational failures) are not evenly distributed between NWFC and NWFA, but occur with a systematically higher frequency in the shear zone at NWFC. At these specific levels *in toto* 2229 (1194 hereof single-bin) instances of data loss were tallied among the 5048 NWFC velocity profiles examined. Analogous results from the NWFA shear zone were 279 and 219, respectively. This discrepancy did not have instrumental causes; a similar investigation of the surface layer (bins 15–20) at the two sites revealed almost identical data-loss statistics.

When discussing possible causes, focus is on data losses from one bin, these cases being most amenable to analysis. The ADCPs were operated in single-ping mode, and hence it appears likely that the data losses arose from high turbulence levels in conjunction with large thermal contrasts giving rise to acoustic returns of such magnitude that the fish-rejection option included in the ADCP signal processing was activated. (Since this state of affairs had not been foreseen, the ADCP software "trigger" was at its default value during the survey.)

An important question is whether single-bin data losses were associated with exceptionally large shears. Evaluated from the two bins adjacent to the one where data loss occurred, the mean lower-bound estimate of the shear

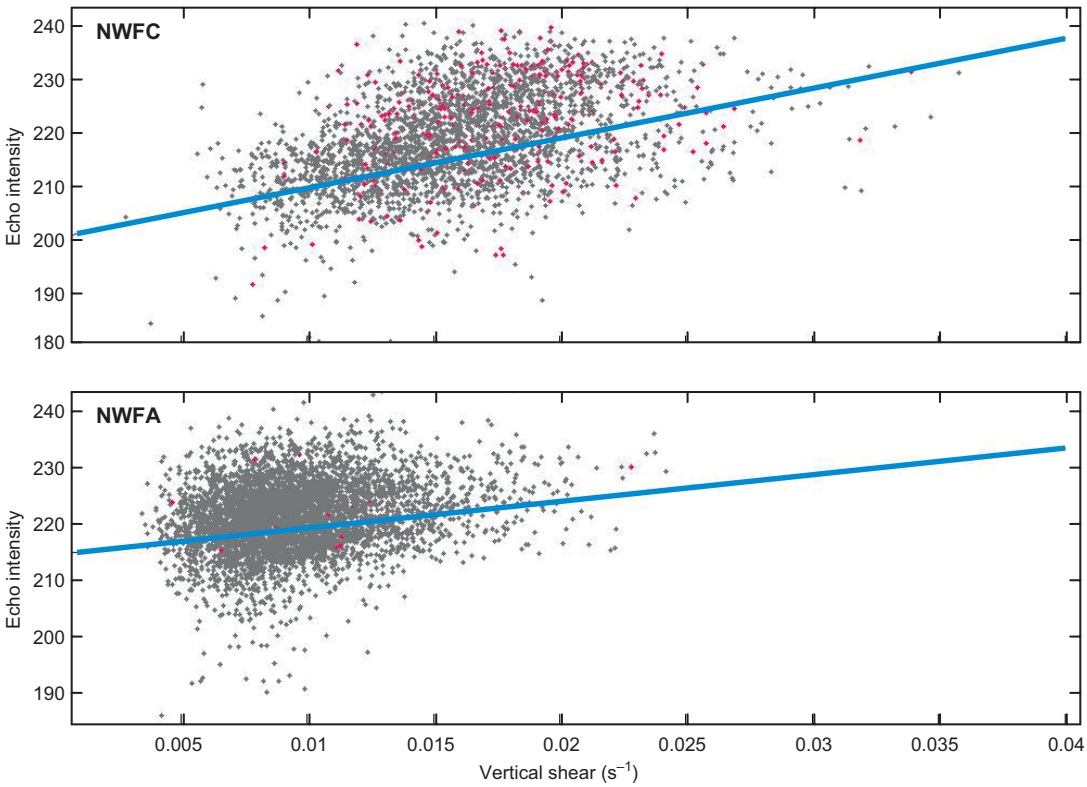

Fig. 7. Maximum vertical shear/"density gradient" *versus* the echo intensity at the same depth and time at the NWFA and NWFC sites. Red dots indicate spatially highly-distinct echo intensities (exceeding 60% of the maximum value found at each station).

was around 0.011 s^{-1}, significantly exceeding the average maximal shear of 0.0068 s^{-1} for "intact" NWFC velocity profiles. A strong shear (and hence also a large flow variance; cf. the lower panel of Fig. 5) is associated with higher and more distinct echo-intensities, which in extreme cases may lead to the above-mentioned data-rejection option being activated (Fig. 7).

Interaction between the bathymetry and the internal tide affecting the shear is here suggested as being the cause of the "excessively turbulent" episodes. This conjecture is supported by experimental investigations from the northern slope of the Wyville-Thomson Ridge (Sherwin 1991) as well as from a site farther upstream in the Faroe-Shetland Channel (Hosegood and van Haren 2003). To judge the plausibility of this suggested mechanism, the temporal distribution of the NWFC shear-zone data losses was investigated. Since a semi-diurnal tide predominates in the Faroe region (Lake and Lundberg 2006), an M_2-window was applied to the 70-day data set. Shear-zone data losses were recorded for each 20-minute phase of the 12.42-hour cycle (*see* black line in Fig. 8). They show a distribution which manifests grossly sinusoidal characteristics, indicating that the number of data losses co-varies with the internal M_2 tide, which in turn affects the shear and consequently also the echo-intensities, cf. the previous paragraph. No co-variation of this type was obtained for a "diurnal window" (*see* red line in Fig. 8 showing the results from a similar analysis for the considerably weaker K_1 tidal constituent). (Note, incidentally, that particulate and/or biological matter would not be expected to manifest any tidal dependence.)

This link between the acoustical observations and the M_2 tidal cycle does not weaken the conjecture that the turbulence giving rise to the refractive-index fluctuations may be shear-induced. Further support for this idea is given

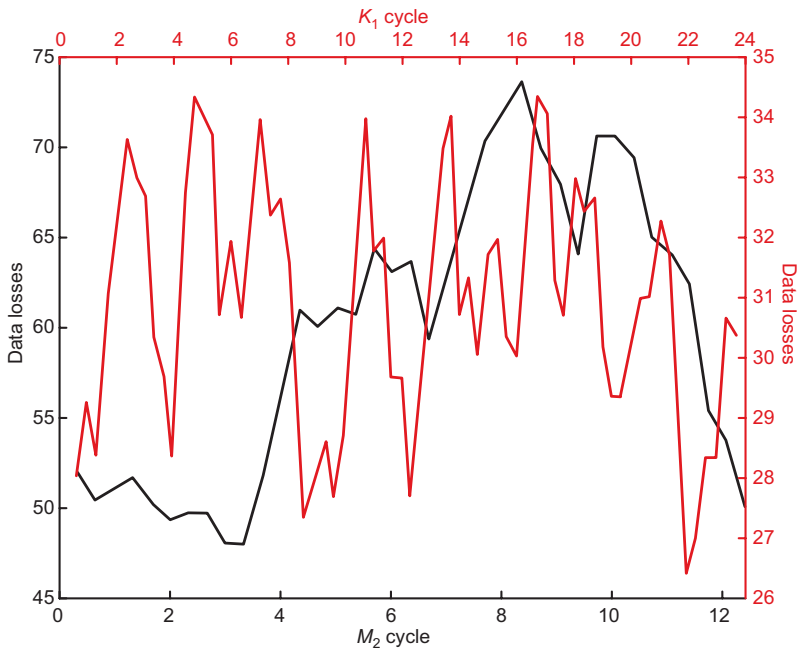

Fig. 8. The shear-zone data-loss distribution over the M_2 tidal period (black line, scale to the left) is seen to crudely reflect this 12.42-hour cycle. The analogous results for the diurnal K_1 cycle (red line, scale to the right) do not show any tidal dependence.

by the fact that on the only occasion when CTD casts were made (at the times of the ADCP deployments), at NWFC the estimated Richardson number was found to have a minimum of approximately 0.28 at the level of maximum vertical shear. Although this estimate is somewhat crude due to the 25-m vertical resolution of the ADCP data, it is in overall agreement with previous results due to Borenäs and Lundberg (1988). As a final caveat it should, however, be underlined that due to the very limited amount of hydrographic data available, the alternative possibility that the turbulence may be caused by breaking internal waves cannot be discounted.

Discussion and conclusions

As previously emphasized, the data set from the Faroe-Bank Channel dealt with here is inappropriate for turbulence studies of the classical type. The flow variance could, however, be interpreted as a proxy for turbulence, and the subsequent analysis of the ADCP records revealed a number of features in favour of this conjecture.

An interesting aspect of the observational records is the marked contrast between conditions at the two sides of the passage. This is caused by the isotherm pinching (Johnson and Sanford 1992, Borenäs *et al*. 2001), which leads to NWFC being characterized by much larger vertical gradients of velocity and density than those encountered at NWFA. The consequences are particularly discernible (*see* Figs. 4 and 7): NWFC manifests considerably more spatially distinct "turbulent" and acoustical properties than NWFA does. The possibly most dramatic result of this difference between the two sides of the passage is the highly skewed distribution of data losses at the NWFC and NWFA sites. The extremely high incidence of shear-zone data loss (~45%) at NWFC appears to be caused by acoustic returns of such strength that the ADCP's fish-elimination option was triggered. These tidally modulated "excessive" echo intensities are caused by turbulence-induced fluctuations of the refractive index, which, due to the strong thermal gradient at NWFC, are particularly pronounced here.

It may be underlined that by using the variance of the flow as a proxy for turbulence, a qualitative picture emerged that yields a consistent relationship between the ADCP-derived velocity and acoustical-return observations in the deeper reaches of the Faroe-Bank Channel. It should, however, be kept in mind that the hydrographic conditions in this passage are highly

unusual, with a very strong thermal stratification and deep-water motion with velocities exceeding 1 m s^{-1} taking place immediately below a comparatively passive surface-water layer of North Atlantic origin. It deserves note, however, that similar exceptional conditions have been encountered in the laboratory, most recently by Cuthbertson *et al*. (2011, 2014) when conducting their experiments on gravity currents in rotating wedge-shaped channels. These investigators ascribed the discrepancy between the experimental observations and their inviscid theoretical predictions to shear-induced turbulence and mixing at the interface between the passive upper layer and the rapidly moving lower layer.

Acknowledgements: The authors thank Prof. Ann-Sofi Smedman and Drs. Heiner Körnich and Thorsten Mauritzen for valuable discussions. This study was supported by the Knut and Alice Wallenberg foundation and the Swedish National Space Board (SNSB). We also wish to thank three anonymous reviewers for constructive comments on a previous version of this manuscript.

References

Borenäs K. & Lundberg P. 1988. On the deep-water flow through the Faroe-Bank Channel. *J. Geophys. Res.* 93(C2): 1281–1292.

Borenäs K. & Lundberg P. 2004. The Faroe-Bank Channel deep-water overflow. *Deep-Sea Res.* II 51: 335–350.

Borenäs K., Lake I. & Lundberg P. 2001. On the intermediate water masses of the Faroe-Bank Channel overflow. *J. Phys. Oceanogr.* 31: 1904–1914.

Cuthbertson A., Laanearu J., Wåhlin A. & Davies P. 2011. Experimental and analytical investigation of dense gravity currents in a rotating, up-sloping and converging channel. *Dyn. Atmos. Oceans* 52: 386–409.

Cuthbertson, A., Lundberg P., Davies P. & Laanearu J. 2014. Gravity currents in rotating, wedge-shaped adverse channels. *Env. Fluid. Mech.*, doi:10.1007/s10652-013.9285-4.

Fer I., Peterson A. & Ullgren J. 2014. Microstructure measurements from an underwater glider in the turbulent Faroe Bank Channel overflow. *J. Atm. Ocean. Tech.* 31: 1128–1150.

Fer I., Voet G., Seim K., Rudels B. & Latarius K. 2010. Intense mixing of the Faroe Bank Channel overflow. *Geophys. Res. Lett.* 37, L02604, doi:10.1029/2009GL041924.

Goodman L. 1990. Acoustic scattering from oceanic microstructure. *J. Geophys. Res.* 95(C7): 11557–11573.

Hansen B. & Østerhus S. 2007. Faroe Bank Channel overflow 1995–2005. *Progr. Oceanogr.* 75: 817–856.

Hosegood P. & van Haren H. 2003. Ekman-induced turbulence over the continental slope in the Faroe-Shetland Channel as inferred from spikes in current meter observations. *Deep-Sea Res.* I 50: 657–680.

Johnson G. & Sanford T. 1992. Secondary circulation in the Faroe Bank Channel outflow. *J. Phys. Oceanogr.* 22: 927–933.

Lake I. & Lundberg P. 2006. Seasonal barotropic modulation of the deep-water overflow through the Faroe-Bank Channel. *J. Phys. Oceanogr.* 36: 2328–2339.

Lake I. Borenäs K. & Lundberg P. 2005. Potential-vorticity characteristics of the Faroe-Bank Channel deep-water overflow. *J. Phys. Oceanogr.* 35: 921–932.

Lorke A. & Wüest K. 2005. Application of coherent ADCP for turbulence measurements in the bottom boundary layer. *J. Atm. Ocean. Tech.* 22: 1821–1828.

Mauritzen C., Price J., Sanford T. & Torres D. 2005. Circulation and mixing in the Faroese Channels. *Deep-Sea Res.* I 52: 883–913.

Nörrevang A., Brattegard T., Josefson A. B., Sneli J.-A. & Tendal O.S. 1994. List of Biofar stations. *Sarsia* 79: 165–180.

Perlin A., Moum J., Klymak J.. Levine M., Boyd T. & Kosro P. 2007. Organization of stratification, turbulence, and veering in bottom Ekman layers. *J. Geophys. Res.* 112, C05S90, doi:10.1029/2004JC002641.

Seim H., Gregg M. & Miyamoto R. 1995. Acoustic backscatter from turbulent microstructure. *J. Atm. Ocean. Tech.* 12: 367–380.

Sherwin T. 1991. Evidence of a deep internal tide in the Faroe–Shetland Channel. In: Parker B.B. (ed.), *Tidal hydrodynamics*, John Wiley, Now York, pp. 469–488.

Thomsen R., Gordon L. & Dymond J. 1989. Acoustic current profiler observations of a mid-ocean ridge hydrothermal plume. *J. Geophys. Res.* 94: 4709–4720.